The ground states and pseudospin textures of rotating two-component Bose–Einstein condensates trapped in harmonic plus quartic potential*

Yan Liu(刘燕) and Su-Ying Zhang(张素英)†

Institute of Theoretical Physics, Shanxi University, Taiyuan 030006, *China*

(Received 27 December 2015; revised manuscript received 26 April 2016; published online 20 July 2016)

The ground states of two-component miscible Bose–Einstein condensates (BECs) confined in a rotating annular trap are obtained by using the Thomas–Fermi (TF) approximation method. The ground state density distribution of the condensates experiences a transition from a disc shape to an annulus shape either when the angular frequency increases and the width and the center height of the trap are fixed, or when the width and the center height of the trap increase and the angular frequency is fixed. Meantime the numerical solutions of the ground states of the trapped two-component miscible BECs with the same condition are obtained by using imaginary-time propagation method. They are in good agreement with the solutions obtained by the TF approximation method. The ground states of the trapped two-component immiscible BECs are also given by using the imaginary-time propagation method. Furthermore, by introducing a normalized complex-valued spinor, three kinds of pseudospin textures of the BECs, i.e., giant skyrmion, coaxial double-annulus skyrmion, and coaxial three-annulus skyrmion, are found.

Keywords: Bose–Einstein condensate, pseudospin texture, skyrmion

PACS: 03.75.Lm, 03.75.Mn **DOI:** 10.1088/1674-1056/25/9/090304

1. Introduction

With the implementation of Bose–Einstein condensates (BECs) in experiments,[1–3] the corresponding theoretical research has also made great progress. For the system of rotating BECs, the topological defects of single component BECs are always quantized vortices. For example, when the single BECs trapped in a harmonic plus quartic potential are driven to rotate, a series of singly quantized vortices will be created. Faster rotation generates more vortices, which finally condense into a giant vortex.[4,5] Different from the single BECs described by the scalar order parameter, the ground states and dynamic behavior of two-component BECs are always described by the vector order parameter.[6,7] With the change of the relative interaction strength between intra-component and inter-component, the two-component BECs can be divided into two kinds: miscible and immiscible. Different trap potential and angular velocity enable more intriguing topological structures.[8–11] In addition, no quantized vortex appears in two-component BECs at sufficiently slow rotations, but its effective velocity is nonzero. Thus in the rotating two-component BECs, there must be other new topological excitations such as skyrmion, giant skyrmion, and so on, which do not exist in single BECs. For two-component immiscible BECs, the spin textures are various for different external potential, s-wave scattering lengths or rotating angular frequency.[12,13] For example, in a harmonic trap, the interface of two components becomes curved for equal particle number but different intra-component scattering lengths, and the component with strong interaction curves towards the one with weak interaction. With the increase of angular frequency, the interface of two components becomes annular and the corresponding spin texture is a giant skyrmion.[14,15] The spin texture can also be coaxial double-annulus skyrmion if two-component immiscible BECs are confined in an annular trap made of harmonic plus linear potential.[16] More interesting phenomena have been presented in spin–orbit coupled BECs.[17–20]

In this paper, we discuss the ground states and the corresponding spin textures of rotating two-component BECs in an annular trap made of harmonic plus quartic potential. The quartic potential can increase the restriction on BECs, in order to study the BEC and its corresponding properties when the rotation speed exceeds the radial harmonic frequency. Firstly, we use the Thomas–Fermi (TF) approximation method to obtain the ground states of two-component miscible BECs for two cases: (i) the angular frequency increases while the width and the center height of the trap are fixed; (ii) the width and the center height of the trap increase while the angular frequency remains the same. Secondly, we make a comparison between the analytical solutions and the numerical solutions which are obtained by the imaginary-time propagation method. Thirdly,

*Project supported by the National Natural Science Foundation of China (Grant Nos. 91430109 and 11404198), the Specialized Research Fund for the Doctoral Program of Higher Education of China (Grant No. 20111401110004), and the Natural Science Foundation of Shanxi Province, China (Grant No. 2014011005-3).

†Corresponding author. E-mail: zhangsy@sxu.edu.cn

© 2016 Chinese Physical Society and IOP Publishing Ltd

we study the ground states and the corresponding pesudospin textures of two-component immiscible BECs by introducing a normalized complex-valued spinor and using the imaginary-time propagation method.

2. Theoretical model

Consider two-component BECs confined in the following annular trap

$$V(r)=\frac{1}{2}\hbar\omega_{\perp}\left[V_0\left(\frac{1}{a_0^2}r^2-r_0\right)^2\right], \tag{1}$$

where $a_0=\sqrt{\hbar/m\omega_{\perp}}$, V_0 and r_0 are dimensionless constants, $r=\sqrt{x^2+y^2}$ is the radial coordinate. The structures of the annular trap for different r_0 are shown in Fig. 1. From Fig. 1(b), we can see that the lowest point of the trap is $(\pm a_0\sqrt{r_0},0)$ and the highest center point of the trap is $(0,\hbar\omega_{\perp}V_0r_0^2/2)$.

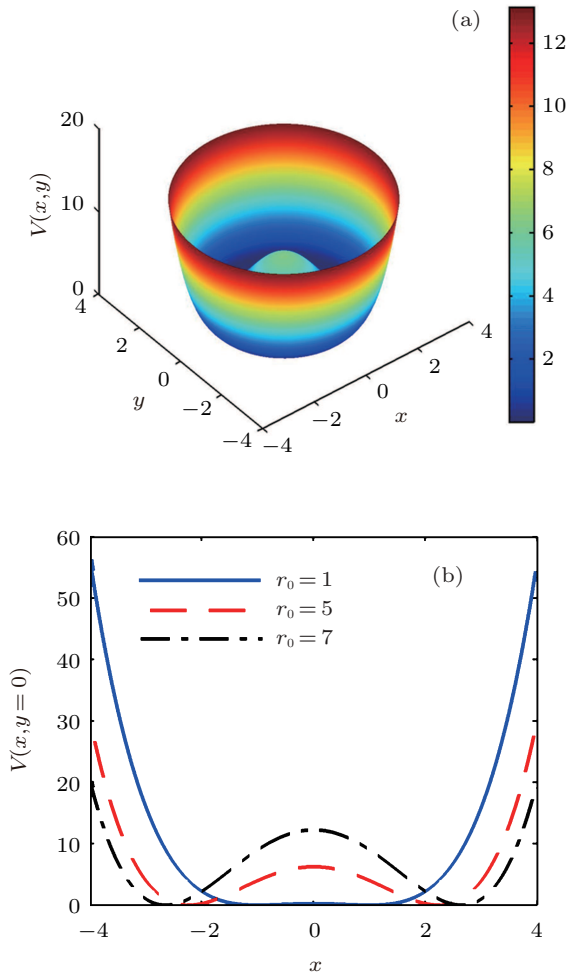


Fig. 1. (color online) (a) Schematic of the annular trapping potential with $V_0=0.5$ and $r_0=5$. (b) The cross sections of $V(r)$ along x with different r_0.

The trapped rotating two-component BECs can be characterized by the vector order parameter $\psi=(\psi_1,\psi_2)^{\mathrm{T}}$, which is governed by the time-dependent coupled Gross–Pitaevskii (GP) equation with angular velocity $\boldsymbol{\Omega}=\Omega\boldsymbol{z}$

$$\begin{aligned}&\mathrm{i}\hbar\frac{\partial\psi_j(\boldsymbol{r},t)}{\partial t}\\&=\left[-\frac{\hbar^2\nabla^2}{2m}+V+\sum_{k=1}^{2}U_{jk}|\psi_k^2|-\Omega L_z\right]\psi_j(\boldsymbol{r},t),\end{aligned} \tag{2}$$

where $U_{jk}=4\pi\hbar^2a_{jk}/m$ $(j,k=1,2)$. When $k=j$, U_{jk} represents the intra-component interaction strength, and when $k\neq j$, U_{jk} represents the inter-component interaction strength. Here a_{jk} is the intra-component $(k=j)$ or inter-component $(k\neq j)$ s-wave scattering length. $L_z=-\mathrm{i}\hbar(x\partial y-y\partial x)$ is the z-component of the angular momentum operator. The wave functions are normalized as

$$\sum_j\int|\psi_j|^2d\boldsymbol{r}=N, \tag{3}$$

where N is the total number of particles in the condensates. After separating the wave function as $\psi_j(\boldsymbol{r},t)=\phi_j(x,y,t)\varphi(z)$ and re-scaling $\tilde{\boldsymbol{r}}=\boldsymbol{r}/a_0$, $\tilde{t}=\omega_{\perp}t$, $\tilde{\psi}_j=(a_0/\sqrt{N})\psi_j$, $\tilde{\Omega}=\Omega/\omega_{\perp}$, and $\tilde{L}_z=L_z/\hbar$, we obtain the quasi-two-dimensional dimensionless coupled GP equations by removing the wavy lines

$$\begin{aligned}\mathrm{i}\frac{\partial\phi_1}{\partial t}&=\left[-\frac{1}{2}\nabla^2+\frac{1}{2}V_0\left(r^2-r_0\right)^2+g_{11}|\phi_1|^2\right.\\&\quad\left.+g_{12}|\phi_2|^2-\Omega L_z\right]\phi_1,\end{aligned} \tag{4}$$

$$\begin{aligned}\mathrm{i}\frac{\partial\phi_2}{\partial t}&=\left[-\frac{1}{2}\nabla^2+\frac{1}{2}V_0\left(r^2-r_0\right)^2+g_{22}|\phi_1|^2\right.\\&\quad\left.+g_{21}|\phi_2|^2-\Omega L_z\right]\phi_2,\end{aligned} \tag{5}$$

where the interaction coefficients are defined as $g_{jk}=4\pi N\eta a_{jk}$, with the reduced parameter $\eta=\int\mathrm{d}z|\varphi(z)|^4/\int\mathrm{d}z|\varphi(z)|^2$. The wave functions are normalized as

$$\sum_j\int|\phi_j|^2\mathrm{d}x\mathrm{d}y=1. \tag{6}$$

Additionally, we make the following assumption:

$$\int(|\phi_1|^2-|\phi_2|^2)\mathrm{d}x\mathrm{d}y=M, \tag{7}$$

where $M\in[0,1)$ is an adjustable parameter. So

$$\int|\phi_1|^2\mathrm{d}x\mathrm{d}y=\frac{1+M}{2}, \tag{8}$$

$$\int|\phi_2|^2\mathrm{d}x\mathrm{d}y=\frac{1-M}{2}. \tag{9}$$

3. Two-component miscible BECs

If the interaction coefficients satisfy $g_{12}^2<g_{11}g_{22}$, the two-component BECs are miscible. We first use an equivalent Lagrangian formalism corresponding to Eqs. (4) and (5) as

$$\mathscr{L}[\phi_1,\phi_2]=\mathscr{T}[\phi_1,\phi_2]-\mathscr{F}[\phi_1,\phi_2], \tag{10}$$

where

$$\mathscr{T}[\phi_1,\phi_2]=\int \mathrm{d}x\mathrm{d}y\left\{\sum_{j=1,2}\left[\frac{\mathrm{i}}{2}\left(\phi_j^*\frac{\partial\phi_j}{\partial t}-\frac{\partial\phi_j^*}{\partial t}\phi_j\right)\right]\right\} \quad (11)$$

is the time-dependent part of the Lagrangian function,

$$\begin{aligned}\mathscr{F}[\phi_1,\phi_2] = &\int \mathrm{d}x\mathrm{d}y\Bigg\{\sum_{j=1,2}\left[\frac{1}{2}|\nabla\phi_j|^2+V|\phi_j|^2\right.\\&+\sum_{k=1,2}\frac{1}{2}g_{jk}|\phi_j|^2|\phi_k|^2-\Omega\mathrm{Re}(\phi_j^*L_z\phi_j)\\&\left.-\mu_j|\phi_j|^2\right]\Bigg\}, \quad (12)\end{aligned}$$

is the free-energy function, and μ_j is a Lagrange multiplier.

3.1. Thomas–Fermi approximation

Using the replacement $\phi_j=\sqrt{\rho_j(\boldsymbol{r},t)}\exp(\mathrm{i}\theta_j(\boldsymbol{r},t))$, we have $|\nabla\phi|^2=|\nabla\sqrt{\rho_j}|^2+|\nabla\theta_j|^2|\phi_j|^2$ and $\rho_j(\boldsymbol{r},t)=|\phi_j(r,t)|^2$. The gradient of the phase $\nabla\theta_j(\boldsymbol{r},t)=\boldsymbol{v}=\boldsymbol{\Omega}\times\boldsymbol{r}$ gives the dimensionless superfluid velocity. For the TF approximation, the curvature of the density $\nabla\sqrt{\rho_j}$ is ignored. In this limit, the variation of the free energy $\mathscr{F}$ with respect to $|\phi_j|^2$ yields

$$g_{11}|\phi_1|^2+g_{12}|\phi_2|^2=\mu_1+\frac{1}{2}\Omega^2r^2-V, \quad (13)$$

$$g_{22}|\phi_2|^2+g_{12}|\phi_1|^2=\mu_2+\frac{1}{2}\Omega^2r^2-V. \quad (14)$$

So we obtain the following TF density of the BECs:

$$|\phi_1|^2=\frac{(g_{22}-g_{12})[-V_0r^4+(\Omega^2+2V_0r_0)r^2-V_0r_0^2]+2(\mu_1g_{22}-\mu_2g_{12})}{2(g_{11}g_{22}-g_{12}^2)}, \quad (15)$$

$$|\phi_2|^2=\frac{(g_{11}-g_{12})[-V_0r^4+\pi(\Omega^2+2V_0r_0)r^2-V_0r_0^2]+2(\mu_2g_{11}-\mu_1g_{12})}{2(g_{11}g_{22}-g_{12}^2)}. \quad (16)$$

3.2. Vortex lattice with central hole

Equation (15) or Eq. (16) allows a direct solution for the "classical" turning points where the TF density vanishes

$$R_{1i}^2=\frac{\Omega^2+2V_0r_0}{2V_0}\pm\sqrt{\left(\frac{\Omega^2+2V_0r_0}{2V_0}\right)^2+\frac{2(\mu_1g_{22}-\mu_2g_{12})-V_0r_0^2(g_{22}-g_{12})}{V_0(g_{22}-g_{12})}}, \quad (17)$$

and

$$R_{2i}^2=\frac{\Omega^2+2V_0r_0}{2V_0}\pm\sqrt{\left(\frac{\Omega^2+2V_0r_0}{2V_0}\right)^2+\frac{2(\mu_2g_{11}-\mu_1g_{12})-V_0r_0^2(g_{11}-g_{12})}{V_0(g_{11}-g_{12})}}, \quad (18)$$

where $i=+,-$ correspond to the $\pm$ appearing on the right-hand side of Eqs. (17) and (18). The plus signs yield the outer squared radius R_{1+}^2 and R_{2+}^2, and the minus signs denote the inner squared radius R_{1-}^2 and R_{2-}^2. We discuss the density profile of ϕ_1 and ϕ_2 in two cases respectively:

Case 1 The width and the center height of the trap are fixed while the angular frequency increases.

The central hole in ϕ_1 first appears when $\mu_1g_{22}-\mu_2g_{12}=V_0r_0^2(g_{22}-g_{12})/2$ (so that $R_{1-}^2=0$ and $R_{1+}^2=(\Omega^2+2V_0r_0)/V_0$). According to the normalization condition (8), the critical rotation frequency $\Omega_{1\mathrm{h}}$, at which the central density of ϕ_1 first vanishes, can be expressed as

$$\Omega_{1\mathrm{h}}^2=-2V_0r_0+\left[\frac{6(1+M)(g_{11}g_{22}-g_{12}^2)}{\pi V_0(g_{22}-g_{12})}\right]^{1/3}V_0. \quad (19)$$

If $\mu_1g_{22}-\mu_2g_{12}<V_0r_0^2(g_{22}-g_{12})/2$, $R_{1-}^2>0$ and squared radius R_{1+}^2 and R_{1-}^2 satisfy the following conditions:

$$R_{1+}^2+R_{1-}^2=\frac{\Omega^2+2V_0r_0}{V_0}, \quad (20)$$

$$\begin{aligned}&R_{1+}^2-R_{1-}^2\\&=2\left\{\left(\frac{\Omega^2+2V_0r_0}{2V_0}\right)^2\right.\\&\left.+\frac{2(\mu_1g_{22}-\mu_2g_{12})-V_0r_0^2(g_{22}-g_{12})}{V_0(g_{22}-g_{12})}\right\}^{1/2}. \quad (21)\end{aligned}$$

The normalization condition (8) yields

$$\pi V_0\left(R_{1+}^2-R_{1-}^2\right)^3=\frac{6(1+M)(g_{11}g_{22}-g_{12}^2)}{g_{22}-g_{12}}. \quad (22)$$

Combining Eq. (19) with Eq. (22), we have

$$R_{1+}^2-R_{1-}^2=\frac{\Omega_{1\mathrm{h}}^2+2V_0r_0}{V_0}, \quad (23)$$

and substituting it into Eq. (21), we obtain

$$\begin{aligned}&\mu_1g_{22}-\mu_2g_{12}\\&=\left\{\frac{1}{2}V_0r_0^2-\frac{1}{8}V_0\left[\left(\frac{\Omega^2+2V_0r_0}{V_0}\right)^2-\left(\frac{\Omega_{1\mathrm{h}}^2+2V_0r_0}{V_0}\right)^2\right]\right\}\\&\times(g_{22}-g_{12}). \quad (24)\end{aligned}$$

It is very easy to get

$$(R_{1+}\mp R_{1-})^2 = \frac{(\Omega_{1h}^2+2V_0r_0)^2}{V_0(\Omega^2+2V_0r_0)\pm V_0\sqrt{(\Omega^2+2V_0r_0)^2-(\Omega_{1h}^2+2V_0r_0)^2}}. \quad (25)$$

Clearly, the area $\pi(R_{1+}^2-R_{1-}^2)$ of the annular condensate ϕ_1 remains constant for all $\Omega>\Omega_{1h}$. The average radius $R\equiv(R_{1+}+R_{1-})/2$ increases and the width $d=R_{1+}-R_{1-}$ decreases with the increase of rotating angular frequency.

The central hole in ϕ_2 first appears when $\mu_2g_{11}-\mu_1g_{12}=V_0r_0^2(g_{11}-g_{12})/2$ (so that $R_{2-}^2=0$ and $R_{2+}^2=(\Omega^2+2V_0r_0)/V_0$). According to the normalization condition (9), the critical angular frequency Ω_{2h}, at which the central density of ϕ_2 vanishes, can be expressed as

$$\Omega_{2h}^2=-2V_0r_0+\left[\frac{6(1-M)\left(g_{11}g_{22}-g_{12}^2\right)}{\pi V_0(g_{11}-g_{12})}\right]^{1/3}V_0. \quad (26)$$

If $\mu_2g_{11}-\mu_1g_{12}<V_0r_0^2(g_{11}-g_{12})/2$, the density profile of ϕ_2 is an annulus and its inner and outer squared radius satisfy the following conditions:

$$R_{2+}^2+R_{2-}^2=\frac{\Omega^2+2V_0r_0}{V_0}, \quad (27)$$

$$R_{2+}^2-R_{2-}^2=2\left\{\left(\frac{\Omega^2+2V_0r_0}{2V_0}\right)^2+\frac{2(\mu_2g_{11}-\mu_1g_{12})-V_0r_0^2(g_{11}-g_{12})}{V_0(g_{11}-g_{12})}\right\}^{1/2}. \quad (28)$$

The normalization condition (9) also yields

$$\pi V_0\left(R_{2+}^2-R_{2-}^2\right)^3=\frac{6(1-M)\left(g_{22}g_{11}-g_{12}^2\right)}{g_{11}-g_{12}}. \quad (29)$$

Combining Eqs. (26) and (29), we have

$$R_{2+}^2-R_{2-}^2=\frac{\Omega_{2h}^2+2V_0r_0}{V_0}. \quad (30)$$

The relationship between the chemical potential and interaction strength is

$$\mu_2g_{11}-\mu_1g_{12}=\left\{\frac{1}{2}V_0r_0^2-\frac{1}{8}V_0\left[\left(\frac{\Omega^2+2V_0r_0}{V_0}\right)^2-\left(\frac{\Omega_{2h}^2+2V_0r_0}{V_0}\right)^2\right]\right\}\times(g_{11}-g_{12}). \quad (31)$$

According to Eqs. (27) and (30), we have

$$(R_{2+}\mp R_{2-})^2 = \frac{(\Omega_{2h}^2+2V_0r_0)^2}{V_0(\Omega^2+2V_0r_0)\pm V_0\sqrt{(\Omega^2+2V_0r_0)^2-(\Omega_{2h}^2+2V_0r_0)^2}}. \quad (32)$$

It is obvious that the area $\pi(R_{2+}^2-R_2^2)$ of the annular condensate ϕ_2 remains constant for all $\Omega>\Omega_{2h}$. The average radius $R\equiv(R_{2+}+R_{2-})/2$ increases and the width $d=R_{2+}-R_{2-}$ decreases with the increase of rotating angular frequency.

Case 2 The angular frequency is fixed while the width and the center height of the trap increase.

Similar to the case 1, we can obtain two critical values of r_0, at which the central density of ϕ_1 or ϕ_2 first vanishes, by

$$r_0^{1h}=-\frac{\Omega^2}{2V_0}+\frac{1}{2}\left[\frac{6(1+M)\left(g_{11}g_{22}-g_{12}^2\right)}{\pi V_0(g_{22}-g_{12})}\right]^{1/3}, \quad (33)$$

$$r_0^{2h}=-\frac{\Omega^2}{2V_0}+\frac{1}{2}\left[\frac{6(1-M)\left(g_{11}g_{22}-g_{12}^2\right)}{\pi V_0(g_{11}-g_{12})}\right]^{1/3}. \quad (34)$$

The change of the annular condensates is the same as case 1 for all $r_0>r_0^{1h}$ or $r_0>r_0^{2h}$.

According to the above analyses and additionally assuming $\Omega_{1h}>\Omega_{2h}$ and $r_0^{1h}>r_0^{2h}$, two-component miscible BECs can present three kinds of structures of the density distributions for different Ω or r_0: (i) if $\Omega_{1h}>\Omega_{2h}>\Omega$ or $r_0^{1h}>r_0^{2h}>r_0$, both components are disc shaped; (ii) if $\Omega_{1h}>\Omega>\Omega_{2h}$ or $r_0^{1h}>r_0>r_0^{2h}$, ϕ_1 is disc shaped and ϕ_2 is annular shaped; (iii) if $\Omega>\Omega_{1h}>\Omega_{2h}$ or $r_0>r_0^{1h}>r_0^{2h}$, both components are annular shaped. When $g_{11}=g_{22}=g$ and $\Omega=1$, $M=0.4$, $V_0=0.5$, $g_{12}=g_{21}=200$, we draw the phase diagram of the ground state density distribution of two-component miscible BECs with the varied r_0 and g in Fig. 2, which shows that the solutions obtained by the above analytic method agree with the numerical solutions. In addition, we take $\Omega=0.5$, $r_0=11$, $V_0=0.5$, $M=0.4$, $g_{11}=g_{22}=1000$, and $g_{12}=g_{21}=800$ to compare the analytic solution with the numerical solution, as shown in Fig. 3.

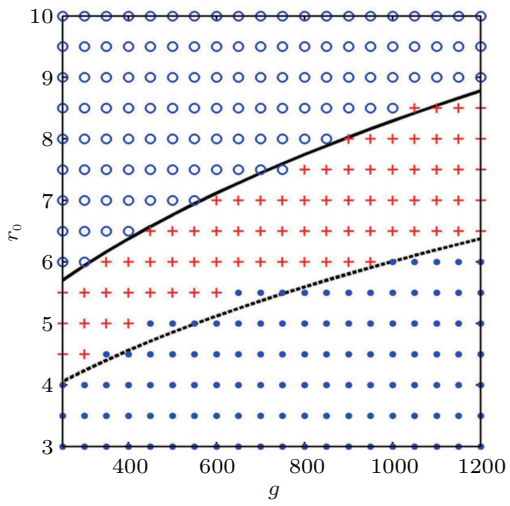


Fig. 2. (color online) r_0–g phase diagram for parameters $\Omega=1$, $M=0.4$, $V_0=0.5$, and $g_{12}=g_{21}=200$. The dashed line indicates the value of r_0^{1h} given by Eq. (33), and the solid line indicates the value of r_0^{2h} given by Eq. (34). The circles indicate that two components are annulus shaped; the plus signs indicate that the density distributions of the big component are disc shaped and the density distributions of the small component are annulus shaped; the points indicate that two components are both disc shaped.

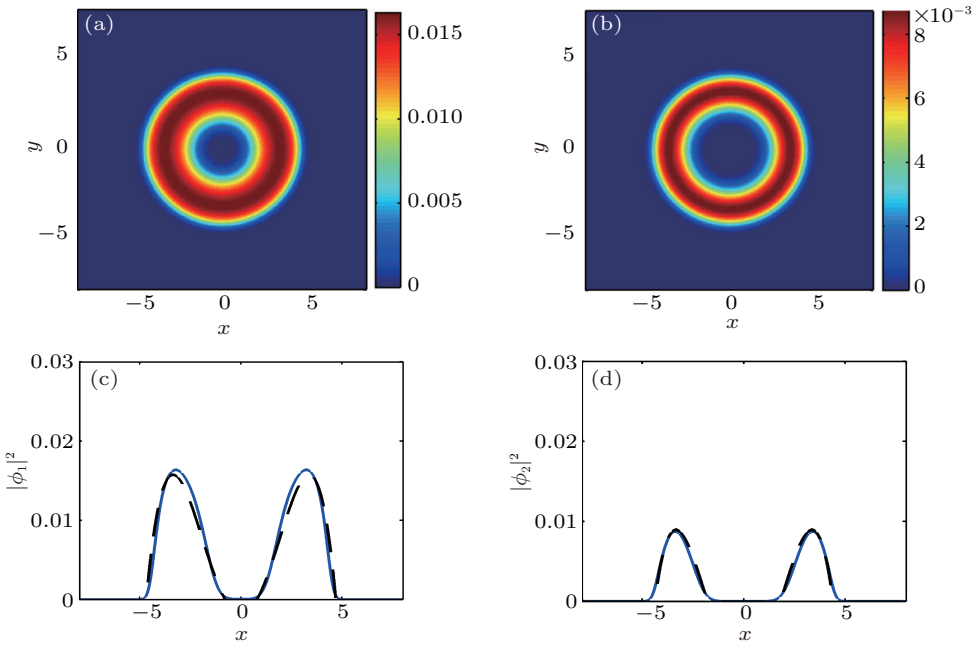


Fig. 3. (color online) (a) The ground state density profile of ϕ_1, (b) the ground state density profile of ϕ_2, (c) the comparison of ϕ_1 (solid line) with the analytic solution (dashed line) of Eq. (15), and (d) the comparison of ϕ_2 (solid line) with the analytic solution (dashed line) of Eq. (16). Here we take $M = 0.4$, $g_{11} = g_{22} = 1000$, $g_{12} = g_{21} = 800$, $\Omega = 0.5$, $r_0 = 11$, and $V_0 = 0.5$.

4. Two-component immiscible BECs

In this section, we illustrate the ground states and the pseudospin textures of two-component immiscible BECs, at which the interaction strength satisfies $g_{12}^2 > g_{11}g_{22}$. Under this condition, the TF approximation is no longer applicable because it fails to describe the domain boundary region, where the quantum pressure term cannot be ignored. However, we can obtain the ground states by using the imaginary-time propagation method.[21]

We take $g_{11} = 600$, $g_{22} = 1000$, $g_{12} = 800$, $M = 0.1$, $V_0 = 0.5$, and $r_0 = 4$. Figure 4 shows that two-component immiscible BECs present three density distributions with the increase of the angular frequency: (i) ϕ_1 is disc shaped and ϕ_2

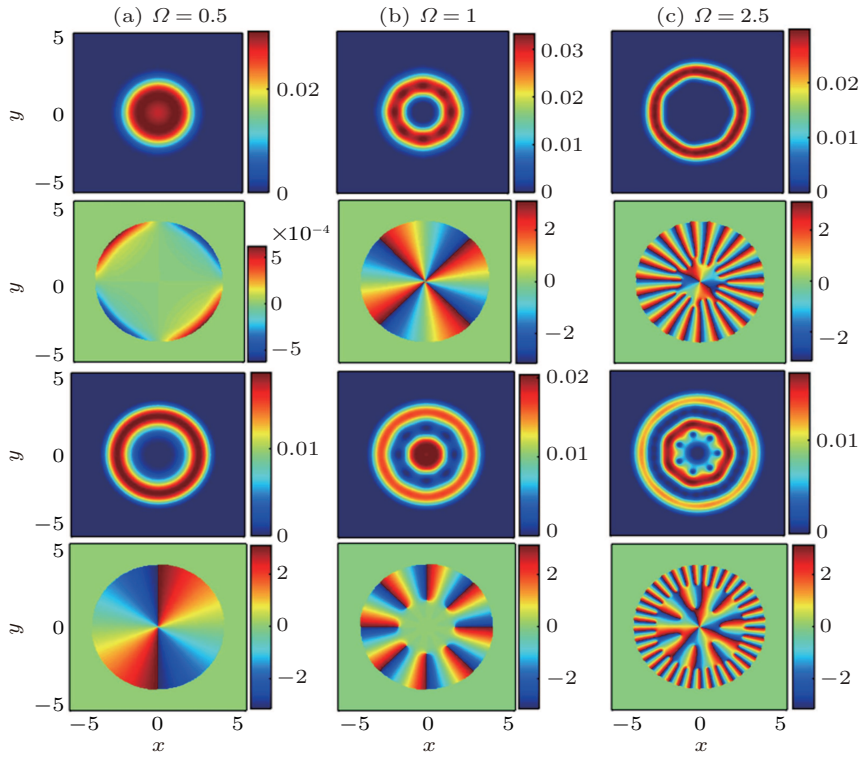


Fig. 4. (color online) The ground state density distributions and phases for different Ω: (a) $\Omega = 0.5$, (b) $\Omega = 1$, and (c) $\Omega = 2.5$. The first and the third rows are the density distributions of ϕ_1 and ϕ_2. The second and the fourth rows are the phases corresponding to the density distributions of the first and third rows, respectively.

is annular shaped; (ii) ϕ_1 is annular shaped and ϕ_2 is a disc plus an annular; (iii) ϕ_1 is annular shaped and ϕ_2 is two annular shaped. The number of the quantum vortex increases with the increase of the angular frequency.

Besides, we take $g_{11} = 600$, $g_{22} = 1000$, $g_{12} = 800$, $M = 0.1$, $V_0 = 0.5$, and $\Omega = 2$. With the increase of the value of r_0, two-component immiscible BECs present three other kinds of density distributions as shown in Fig. 5: (i) ϕ_1 is a disc plus an annulus and ϕ_2 is double annuli; (ii) ϕ_1 is an annulus and ϕ_2 is a disc plus an annulus; (iii) ϕ_1 is an annulus and ϕ_2 is double annuli. The bigger the value of r_0 is, the greater the quantum vortices become.

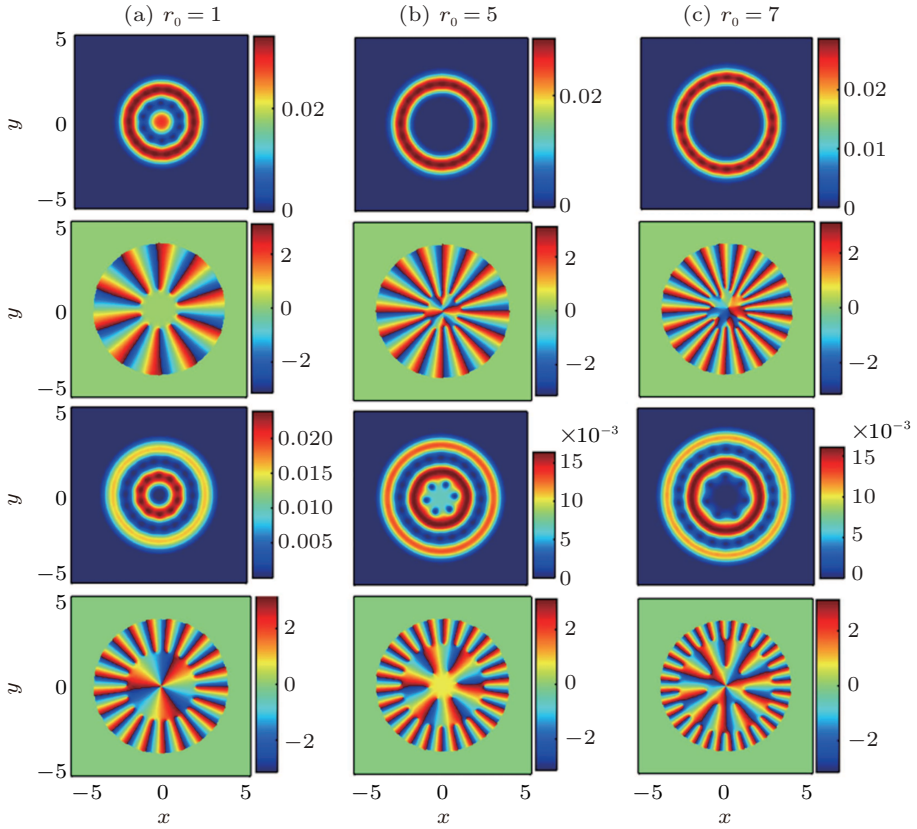


Fig. 5. (color online) The ground state density distributions and phases for different r_0: (a) $r_0 = 1$, (b) $r_0 = 5$, (c) $r_0 = 7$. The first and the third rows are the density distributions of ϕ_1 and ϕ_2. The second and the fourth rows are the phases corresponding to the density distributions of the first and third rows, respectively.

In addition, we can introduce the pseudospin concept to study the corresponding pseudospin textures. Using a pseudospin-1/2 BECs to analysis this system, we introduce a normalized complex valued spinor $\chi(r) = [\chi_1(r), \chi_2(r)]^{\mathrm{T}} = [|\chi_1|e^{i\theta_1}, |\chi_2|e^{i\theta_2}]^{\mathrm{T}}$, where $|\chi_1|^2 + |\chi_2|^2 = 1$, θ_j represents the phase of wave function ϕ_j, and $\phi_j = \sqrt{\rho_j(r)}\chi_j(r)$. The pseudospin density is defined as $S = \bar{\chi}(r)\sigma\chi(r)$, where σ is the Pauli matrix. The pseudospin density can be expressed as

$$\begin{cases} S_x = 2|\chi_1||\chi_2|\cos(\theta_1 - \theta_2), \\ S_y = -2|\chi_1||\chi_2|\sin(\theta_1 - \theta_2), \\ S_z = |\chi_1|^2 - |\chi_2|^2. \end{cases} \tag{35}$$

Clearly, the modulus of the total spin is $|S| = \sqrt{S_x^2 + S_y^2 + S_z^2} = 1$. The spin of ϕ_1 points up and the spin of ϕ_2 points down. For the parameters used in Fig. 4, the corresponding pseudospin density distributions S_x, S_y, and S_z are given in Fig. 6. Here, the red represents the spin pointing up and the blue represents the spin pointing down. At the interface of the two components, the spin turns from pointing up to pointing down or from pointing down to pointing up periodically. The period of the annular pseudospin texture is equivalent to that of the corresponding relative phase, because the pseudospin density is just a periodic function of their relative phase. With the increase of the angular velocity, the spin texture changes from giant skyrmions to coaxial double-annulus skyrmion.

In addition, for the parameters used in Fig. 5, the corresponding pseudospin density distributions S_x, S_y, and S_z are given in Fig. 7. With the increase of the value of r_0, the corresponding pseudospin texture changes from coaxial three-annulus skyrmion, which has not been observed or studied in an annular potential and could not exist in harmonic trapping potentials, to coaxial double-annulus skyrmion. The period of the annular pseudospin texture is equal to that of the relative phase of two components.

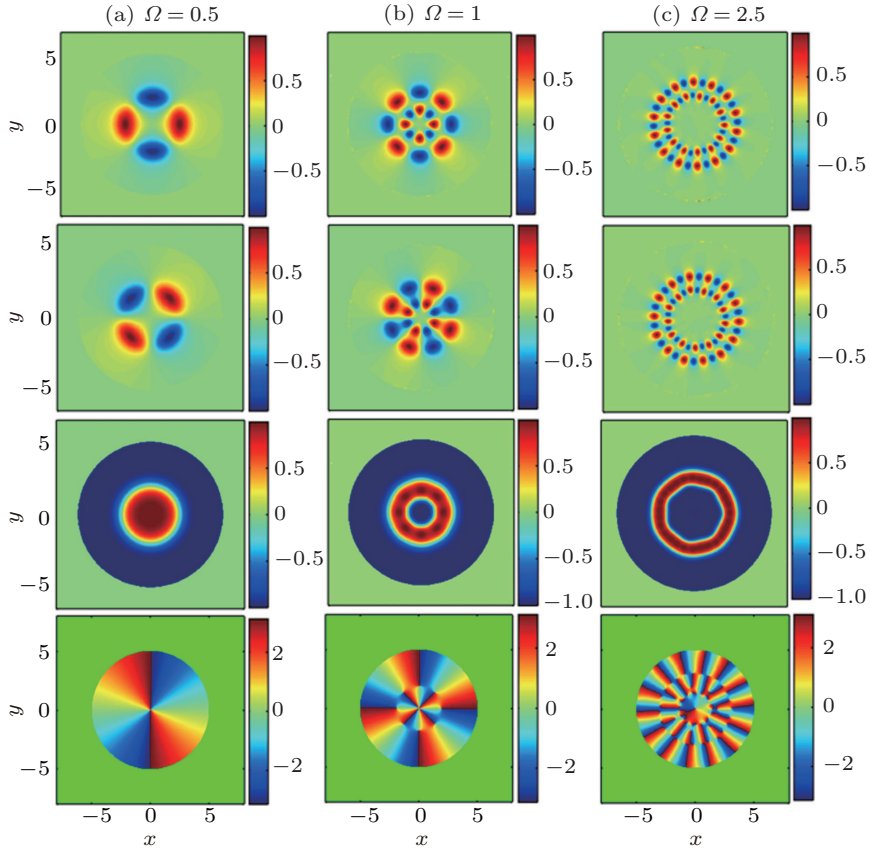


Fig. 6. (color online) The pseudospin densities distributions and the relative phases for different Ω: (a) $\Omega = 0.5$, (b) $\Omega = 1$, and (c) $\Omega = 2.5$. The first row is S_x, the second row is S_y, the third row is S_z, and the fourth row is the relative phases $\theta_1 - \theta_2$.

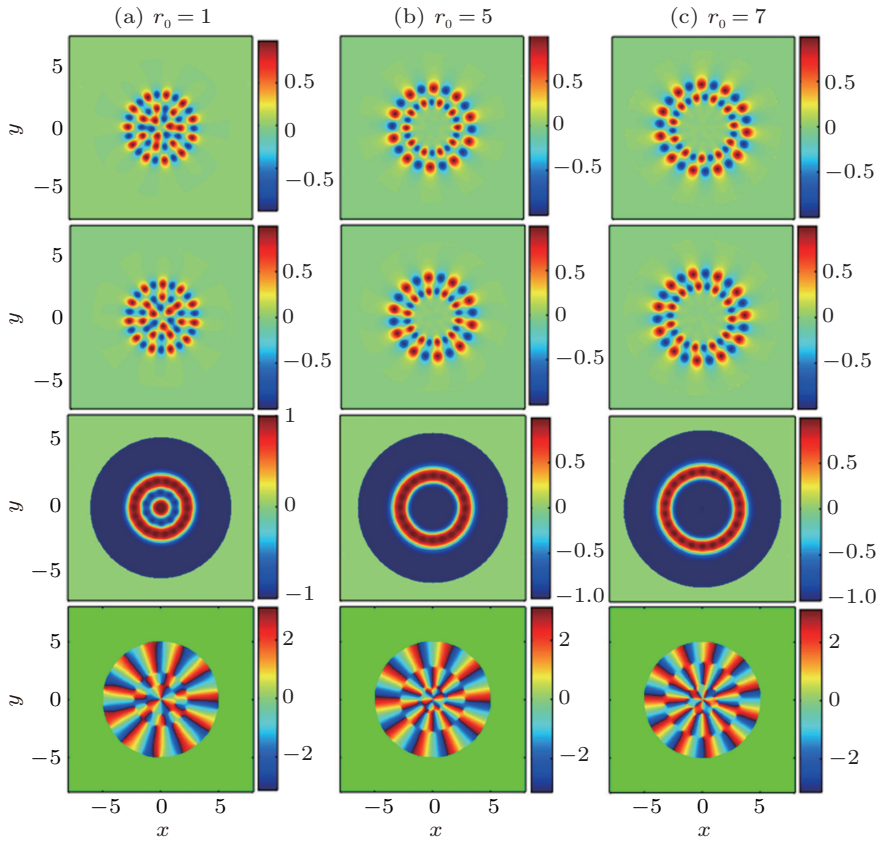


Fig. 7. (color online) The pseudospin densities distributions and the relative phases for different r_0: (a) $r_0 = 1$, (b) $r_0 = 5$, and (c) $r_0 = 7$. The first row is S_x, the second row is S_y, the third row is S_z, and the fourth row is the relative phases $\theta_1 - \theta_2$.

5. Conclusion

We have studied the ground states of two-component miscible BECs analytically and numerically. With the increase of the angular velocity, or with the increase of the central height and width of the external trap potential, two-component miscible BECs present three kinds of density distributions. In addition, we have also investigated the ground states and the spin textures of two-component immiscible BECs. By projecting the system into a pesudospin space, we found a new pesudospin texture, i.e., coaxial three-annulus skyrmion. The period of the annular pseudospin texture of the BECs is equal to that of the relative phase of the two different components.

Furthermore, the TF radius of the two-component miscible BECs confined in the dimensionless harmonic plus quartic potential as $V(r) = \frac{1}{2}V_0(r^2 - r_0)^2$ discussed in this paper, is of convergence under any parameter conditions. But the BEC confined in the dimensionless annular potential as $V(r) = \frac{1}{2}V_0(r - r_0)^2$ [16] has TF radius of convergence only under the condition $\Omega^2 < V_0$.

References

[1] Anderson M A, Ensher J R, Matthews M R, Wieman C E and Cornell E A 1995 *Science* **269** 198

[2] Davis K B, Mewes M O, Andrews M R, Druten N J, Durfee D S, Kurn D M and Ketterle W 1995 *Phys. Rev. Lett.* **75** 3969

[3] Bradley C C, Sackett C A, Tollett J J and Hulet R G 1995 *Phys. Rev. Lett.* **75** 1687

[4] Fetter A L, Jackson B and Stringari S 2005 *Phys. Rev. A* **71** 013605

[5] Kim J K and Fetter A L 2005 *Phys. Rev. A* **72** 023619

[6] Hall D S, Matthews M R, Ensher J R, Wieman C E and Cornell E A 1998 *Phys. Rev. Lett.* **81** 1539

[7] Stenger J, Inouye S, Stamper-Kurn D M, Miesner H J, Chikkatur A P and Ketterle W 1998 *Nature* **396** 345

[8] Mason P and Aftalion A 2011 *Phys. Rev. A* **84** 033611

[9] Kasamatsu K, Tsubota M and Ueda M 2005 *Phys. Rev. A* **71** 043611

[10] Han W, Zhang S Y, Jin J J and Liu W M 2012 *Phys. Rev. A* **85** 043626

[11] Zhang X F, Zhang P, Chen G P, Dong B, Tan R B and Zhang S G 2015 *Acta Phys. Sin.* **64** 060302 (in Chinese)

[12] Liu Y H and Li Y Q 2015 *Chin. Phys. B* **24** 017506

[13] Jia W, Dou F Q, Sun J A and Duan W S 2015 *Chin. Phys. B* **24** 040307

[14] Yang S J, Wu Q S, Zhang S N and Feng S P 2008 *Phys. Rev. A* **77** 033621

[15] Jin J J, Zhang S Y and Han W 2011 *J. Phys. B-At. Mol. Opt. Phys.* **44** 165302

[16] Jin J J, Zhang S Y, Han W and Wei Z F 2013 *J. Phys. B-At. Mol. Opt. Phys.* **46** 075302

[17] Zhang X F, Dong R F, Liu T, Liu W M and Zhang S G 2012 *Phys. Rev. A* **86** 063628

[18] Liu C F and Liu W M 2012 *Phys. Rev. A* **86** 033602

[19] Liu C F, Fan H, Zhang Y C, Wang D S and Liu W M 2012 *Phys. Rev. A* **86** 053616

[20] Chen G P 2015 *Acta Phys. Sin.* **64** 030302 (in Chinese)

[21] Antoine X, Bao W and Besse C 2013 *Comput. Phys. Commun.* **184** 2621